Triboelectric Charging Sequence Induced by Surface Functionalization as a Method To Fabricate High Performance Triboelectric Generators

Sung-Ho Shin,[†] Yang Hyeog Kwon,[†] Young-Hwan Kim,[†] Joo-Yun Jung,[‡] Min Hyung Lee,[*,§] and Junghyo Nah[*,†]

[†]Department of Electrical Engineering, Chungnam National University, Daejeon 305-764, Korea, [‡]Department of Nano Manufacturing Technology, Korea Institute of Machinery and Materials, Daejeon 305-343, Korea, and [§]Department of Applied Chemistry, Kyung Hee University, Yongin, Gyeonggi 446-701, Korea

ABSTRACT Two different materials, apart from each other in a triboelectric series, are required to fabricate high performance triboelectric generators (TEGs). Thus, it often limits the choices of materials and causes related processing issues for TEGs. To address this issue, we report a simple surface functionalization method that can effectively change the triboelectric charging sequence of the materials, broadening material choices and enhancing the performance of TEGs. Specifically, we functionalized the surfaces of the polyethylene terephthalate (PET) films either with poly-L-lysine solution or trichloro(1*H*,1*H*,2*H*,2*H*-perfluorooctyl) silane (FOTS). Consequently, the PET surfaces were modified to have different triboelectric polarities in a triboelectric series. The TEGs, fabricated using this approach, demonstrated the maximum $V_{open\text{-}circuit}$ (V_{oc}) of ~330 V and $J_{short\text{-}circuit}$ (J_{sc}) of ~270 mA/m^2, respectively, at an applied force of 0.5 MPa. Furthermore, the functionalized surfaces of TEGs demonstrated superior stability during cyclic measurement over 7200 cycles, maintaining the performance even after a month. The approach introduced here is a simple, effective, and cost-competitive way to fabricate TEGs, which can also be easily adopted for various surface patterns and device structures.

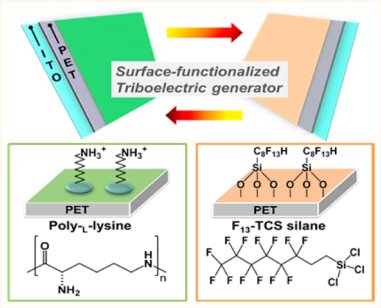

KEYWORDS: triboelectric generator · surface functionalization · solution-derived process · energy harvesting

Energy harvesting using renewable, sustainable, and environmentally friendly resources has gained considerable attention as a viable route to meet rapidly increasing energy demands, initiated in part by quickly growing number of portable electronics.[1−3] Among various sustainable energy resources existing in our living environment, the physical movements originated from various stimuli are one of the highly affordable and reliable energy resources, less affected by external weather conditions.[4−7] The electromagnetic,[8−10] piezoelectric,[11−15] and triboelectric[16,17] effects have been widely employed to convert them into electrical energy. The triboelectric generators (TEGs) harvest energy using triboelectric effect, where electricity is generated by contact-electrification: the charge transfer process is built up when the two material surfaces with opposite triboelectric polarity are in contact with each other.[18,19] The TEG produces high output power density and is especially attractive due to its simple and low-cost device fabrication process.[20,21] To date, many efforts have been made to maximize the output power of the TEGs for the realization of self-powered electronics devices.[22] Most attempts so far have been focused on developing different surface patterning methods[23−26] and novel device structures.[27−31] These efforts, however, were often hindered by limited material combinations available in a triboelectric series and related processing issues. Thus, it will be substantially useful if there is a simple method to render the triboelectric charging sequence of the materials' surfaces, which can expand material choices and improve the performance of the TEGs.

Here we report a simple surface functionalization method that can effectively change the triboelectric sequence of the materials in a triboelectric series, which in turn greatly improves the output performance of

* Address correspondence to minhlee@khu.ac.kr, jnah@cnu.ac.kr.

Received for review March 2, 2015 and accepted April 6, 2015.

Published online April 06, 2015
10.1021/acsnano.5b01340

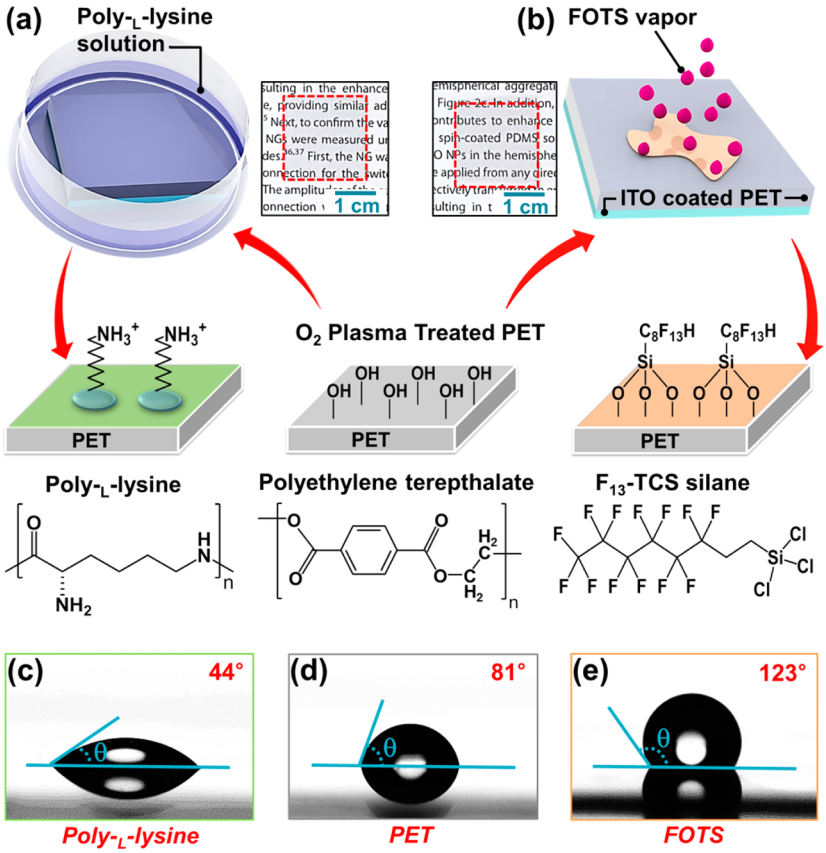

Figure 1. (a and b) Schematic representation of the surface functionalization process. The PET/ITO substrates were treated in oxygen plasma prior to the surface functionalization, rendering strong covalent bond to target molecules. (a) The plasma treated PET surface is functionalized with poly-L-lysine solution by dip-coating, rendering positively charged surface. (b) The plasma treated PET surface is functionalized with FOTS by vapor-phase self-assembling deposition, charging the surface negatively. As-fabricated substrates are transparent. (c–e) Water contact angle measurement for verification of the functionalized surfaces (c) The small contact angle (θ = 44°) shows the effect of positively charged poly-L-lysine coating. (d) Contact angle (θ = 81°) of the nonfunctionalized PET surface. (e) The large contact angle (θ = 123°) shows hydrophobic surface formed by FOTS coating.

the TEGs. Specifically in this work, we functionalized the surface of polyethylene terephthalate (PET) films either with poly-L-lysine or trichloro(1*H*,1*H*,2*H*,2*H*-perfluorooctyl) silane (FOTS) by dip-coating and self-assembling deposition, respectively. As a result, the PET surface functionalized with poly-L-lysine shows positively charged state and the one functionalized with FOTS indicates negatively charged state, exhibiting opposite triboelectric polarity when they are in contact with each other. The TEG fabricated using these functionalized surfaces demonstrated the maximum $V_{open\text{-}circuit}$ (V_{oc}) of ~330 V and $J_{short\text{-}circuit}$ (J_{sc}) of ~270 mA/m^2 when the two flat surfaces are periodically contacted at an applied force of 0.5 MPa. It was ~4 orders of magnitude higher output power in comparison to the one obtained from the TEG with nonfunctionalized surfaces. Besides, the surface functionalized TEGs demonstrated superior stability over 7200 cyclic contact measurement, maintaining the performance even after a month. The approach introduced here is simple, effective, and cost-competitive way to fabricate TEGs, which can also be easily applied to the devices with various surface patterns and device structures.

RESULT AND DISCUSSION

The PET surface functionalization processes are schematically illustrated in Figure 1a,b. Here we note that identical indium tin oxide (ITO)-coated PET substrates were used in this study to demonstrate the roles of surface functionalization. The detailed surface functionalization process can be described as follows. First, ITO-coated PET substrates, precleaned with acetone, IPA, and deionized (DI) water, were treated in oxygen plasma for 100 s, which forms reactive chain ends with hydroxyl (–OH) group strongly binding on the PET surfaces.[32,33] The hydroxyl (–OH) groups on the PET surface are in turn covalently bonded with functionalizing target molecules. Thus, oxygen plasma treatment plays a key role in maintaining reliable output performance during long cyclic measurements even after a month. Next, the plasma treated hydroxyl-PET (H-PET) substrate was soaked in a glass container containing poly-L-lysine solution for 5 min to functionalize the surface [Figure 1a]. Subsequently, the H-PET was washed with DI water and N_2 blow-dried. As depicted in Figure 1a, the poly-L-lysine-coated PET

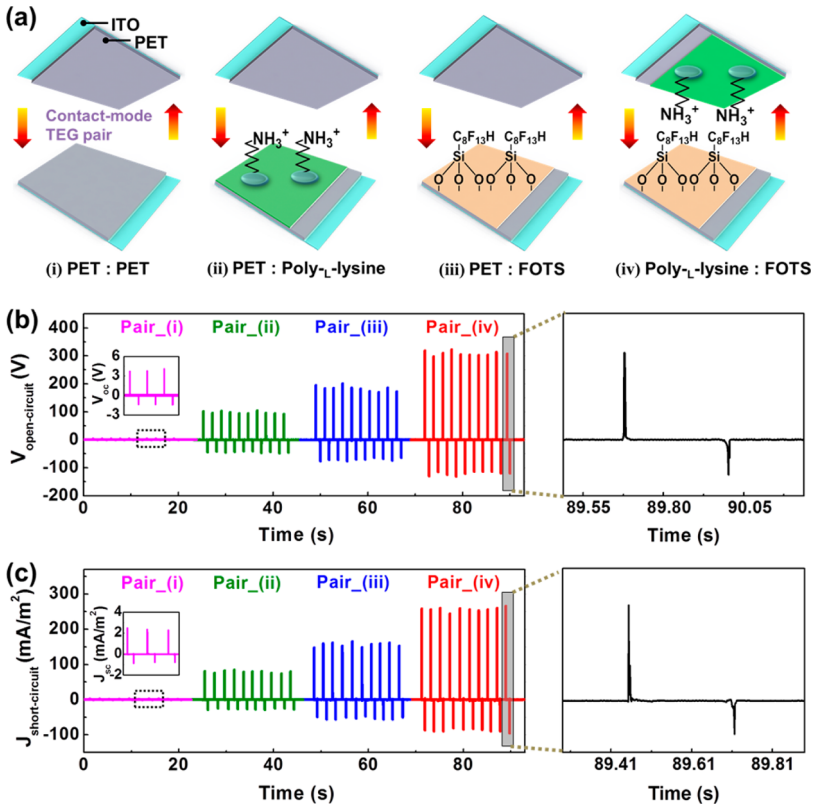

Figure 2. (a) The prepared contact pairs of the TEGs. (i) PET:PET, (ii) PET:P-PET, (iii) PET:F-PET, and (iv) P-PET:F-PET. (b) Open-circuit voltages of the TEGs with different contact pairs. The generated output voltages increase from ~4 V in the device with PET:PET contact pair to ~330 V in the device with (iv) P-PET:F-PET pair. (c) Short-circuit current densities of the same TEGs measured in (b) demonstrates a similar trend as in (b), where the current densities increase from ~2.6 to ~270 mA/m^2 as both surfaces are functionalized. Note: identical experimental conditions were a used in all TEGs. The size of TEGs used was 4 cm^2.

(P-PET) surface is positively charged by amino ($-NH_3^+$) end groups, which are the side chain of the lysine. Lastly, the other substrate was placed in a sealed glass container with a few drops of trichloro(1*H*,1*H*,2*H*,2*H*-perfluorooctyl) silane (FOTS) and then the container was kept in an oven for 95 °C for 1 h [Figure 1b]. During thermal treatment, the H-PET surface is modified by self-assembling chemical vapor phase reaction[34] between the hydroxyl groups and FOTS head groups ($-Cl$). We verified the functionalized surfaces by analyzing water contact angles (θ) by the static sessile drop method. As shown in Figure 1c, when a water droplet is in contact with the P-PET surface, the small contact angle (θ = 44°) was observed between a water droplet and P-PET surface, indicating hydrophilic property (0° < θ < 90°). The small θ is attributed to positively charged amino groups ($-NH_3^+$) with high surface energy,[35,36] where the NH_3^+ molecules interact with the polar hydrogen bond of water molecules by the chemical attractive force, spreading the water droplet. We note that the measured contact angle of P-PET surface is obviously smaller than that (θ = 81°) of nonfunctionalized PET surface [Figure 1d]. In contrast, the hydrophobic property (θ = 123°) was observed in FOTS-functionalized PET (F-PET) surface [Figure 1e]. It is due to the contribution of nonpolar ($-CF_3$) end groups in FOTS with low surface energy.[37]

Next, we prepared four different TEG combinations to systematically investigate and experimentally verify if the generated output performance is indeed induced by the surface functionalization. As shown in the schematic representations [Figure 2a], the contact-mode TEGs with four different functionalization pairs were prepared: (i) PET:PET, (ii) PET:P-PET, (iii) PET:F-PET, and (iv) P-PET:F-PET. With the use of these devices, the open-circuit voltage (V_{oc}) and short-circuit current density (J_{sc}) of the device were measured [Figure 2b,c]. Figure 2b presents the V_{oc} of the four TEGs during cyclic pushing and releasing using a push machine. We note that the experimental conditions and the dimensions of the TEGs were identical, where the device's area is 4 cm^2 and an applied force normal to the surface of the device is 0.5 MPa. Under the forward connection mode, the smallest V_{oc} (~4 V) was measured in the device with (i) PET:PET contact pair [Enlarged view in Figure 2b]. The weak output voltages were still generated between the same PET pair, which may be attributed to the capacitance change between top and bottom electrodes during the cyclic contact motions. After functionalizing one of the TEG surfaces with poly-L-lysine [(ii) PET:P-PET pair], the V_{oc} is immediately

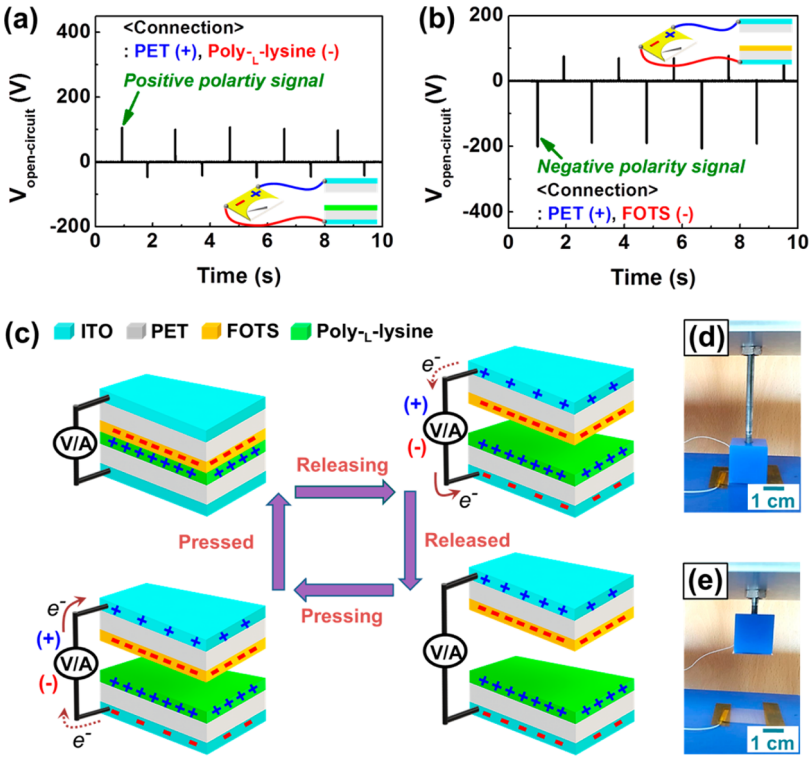

Figure 3. (a) Positive voltage pulses from the TEG consisting of the PET/ITO as the top layer and poly-L-lysine/PET/ITO as the bottom layer. (b) Negative voltage pulses from the TEG consisting of nonfunctionalized PET/ITO as the top layer and FOTS/PET/ITO as the bottom layer. Note: the connection configuration to the measurement instrument was kept the same for both TEGs, where the positive input (+) of the measurement setup is connected to the top electrode and the negative input (−) is connected to the bottom electrode (insets). (c) Power generation mechanism of the TEG with F-PET:P-PET contact pair. When the two surfaces are contacted, the triboelectric charges are built up: positive charges on poly-L-lysine coated surface and negative charges on FOTS treated surface. As the two surfaces start to separate, electrons are driven to flow from the top to the bottom through an external load. When they are completely separated, the charge transfer is finished as the potential difference vanishes. As the two surfaces are pressed toward each other, the transferred electrons flow back in a reverse direction to balance potential difference between the two electrodes. (d) The TEG at the contacted state and (e) separated state mounted on the measurement stage.

increased to ~110 V. In the TEG fabricated with (iii) PET:F-PET pair, where only one surface is functionalized with FOTS, the V_{oc} reaches up to ~205 V. Lastly, the maximum output V_{oc} of ~330 V was obtained using TEG with (iv) P-PET:F-PET contact pair, which is ~80-fold higher by comparison to the V_{oc} measured in (i) PET:PET pair. The measured short-circuit current densities showed a similar trend as the voltage outputs, elevating from the lowest ~2.6 mA/m^2 in the TEG with (i) PET:PET pair to the highest ~270 mA/m^2 in the TEG with (iv) P-PET:F-PET pair [Figure 2c]. Consequently, the output power density has increased by approximately 4 orders of magnitude after functionalizing both surfaces with opposite polarity. The validity of the output signals was also confirmed using switching polarity test, where V_{oc} and J_{sc} are measured by reversely connecting the TEG, and the same the peak to peak magnitude of the outputs voltage with inverted signal polarity was observed [Supporting Information Figure S1]. The output performance enhancement in surface functionalized TEGs can be explained as follows. In the TEG with (ii) PET:P-PET pair, when the PET surface is in contact with the positively charged P-PET surface, the positive charges on the P-PET surface augment potential difference between the two ITO electrodes, increasing output values. Similarly, in the case of (iii) PET:F-PET paired TEG, the F-PET surface is partially negatively charged, induced by the fluorine (F) in the ($-CF_3$) end groups of FOTS. It causes the potential difference between the electrodes as the two surfaces (PET:F-PET) are contacting each other. We note that the fluorinated polymer is well-known as the best electron-accepting material due to its superior electronegativity. Thus, the triboelectric sequence difference between the PET and the F-PET surfaces is relatively larger compared to that between PET and P-PET pair, resulting in higher peak-to-peak output pulses. As expected, the maximum output pulses were obtained in the TEG with (iv) P-PET:F-PET combination, originated from highest potential difference between the two surfaces during cyclic contact motions.

Since the functionalized surfaces of P-PET and F-PET have different polarities, it is necessary to confirm if they are indeed reflected in the output signals and how the surface charge polarity affects the output signals. The Figure 3, panels a and b, respectively, show the

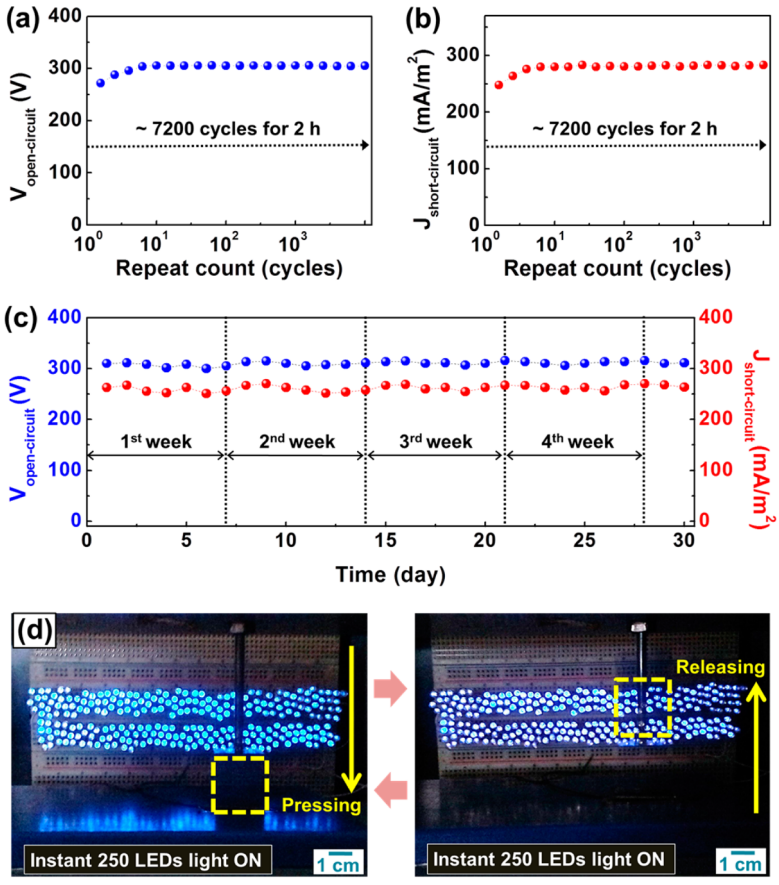

Figure 4. (a) Open-circuit voltage and (b) short-circuit current density measurement for 7200 cycles, revealing the superior mechanical durability and stability of the functionalized surface. (c) Reproducibility test of the same TEG over a month. The TEG was repeatedly measured for 7200 cycles per each week over a month. No performance degradation was observed even after a month. (d) Photographs showing the direct lighting of 250 LEDs during pressing/releasing motions of the TEG fabricated with P-PET:F-PET contact pair.

output pulses of the TEGs with PET:P-PET pair and PET:F-PET pair, exhibiting opposite polarity. Here, the connection configuration to the measurement instrument was kept the same for both TEGs, where top sides are connected to the positive input (+) and the functionalized bottom sides are connected to the negative input (−) of the measurement setup [schematic drawings in Figure 3a,b]. During the contact and retraction motions, the generated output V_{oc} of the PET:P-PET paired TEG shows positive signals [Figure 3a]. On the other hand, the generated output V_{oc} of the TEG with PET:F-PET paired shows negative signals [Figure 3b]. The surface functionalization effect is indeed reflected in the output signals. Therefore, the maximum output voltage observed in the TEG with P-PET:F-PET pair [Figure 2b(iv)] is simply the addition of these output voltages with opposite polarity. To substantiate the results, we also measured the output voltages of the TEGs with F-PET:H-PET pair. Since the hydroxyl (−OH) coated PET surface also retains negatively charged state, negative voltage pulses were generated in the TEG with PET:H-PET pair [Supporting Information Figure S2(a)]. Hence, the V_{oc} of the TEG with F-PET:H-PET pair was reduced since both surfaces possess the same surface polarity [Supporting Information Figure S2(b)]. The power generation mechanisms are schematically described in Figure 3c, using the contact-mode TEG with P-PET:F-PET pair. When the two inner surfaces are brought into contact by the push machine as shown in Figure 3d, the potential difference is induced between them due to the charge transfer, charging P-PET surface more positively and F-PET surface more negatively. As the two surfaces with opposite charges separate [Figure 3e], these opposite triboelectric charges induce a potential difference across the top and bottom electrodes. Therefore, the electrons will be driven to flow from the top to the bottom electrode through an external load until the potential difference between the two electrodes vanishes, producing positive electric current pulse of a half cycle. Next, when the two separated surfaces move toward each other again to a contact mode, the potential difference will be disappeared and transferred electrons will flow back to the top ITO electrode through an external load, generating electrical current pulse in a reverse direction. This process will continue during the cyclic pressing and releasing motion, generating the alternating current (AC).

The stability of the TEG was also examined under periodic contact mode over 7200 cycles for 2 h [Figure 4a,b]. The consistent output performance was observed without any performance degradation during the test, confirming the superior stability of the surface functionalized TEG. We note that similar test results were observed in multiple devices. In addition, the tested TEG was repeatedly measured over 4 weeks and there was no performance degradation [Figure 4c]. We assume that the hydroxy1 (−OH) end groups formed on the PET surface after oxygen plasma treatment provide the strong covalent bonds to the poly-L-lysine and FOTS, maintaining stability of the device even after the applied stresses over long period time.

For visual demonstration of the output power generation, we attempted to drive the commercial light-emitting-diodes (LEDs) through a bridge rectifier which converts the AC into DC signals. The rectified output V_{oc} and J_{sc} of the TEG with P-PET:F-PET contact pair are shown [Supporting Information Figure S3]. The power delivered from the TEG during pressing and releasing motions was sufficient to directly turn on 250 blue LEDs without charging capacitors [Figure 4d and Supporting Information Video 1]. On the other hand, no LEDs were turned on by the TEG with PET: PET contact pair. This result elucidates the compelling role of surface functionalization as a route to render triboelectric charging sequence.

CONCLUSION

In summary, we have developed a surface functionalization method that can effectively modify triboelectric charging sequence. Positively and negatively charged surface states were readily obtained by dip-coating and self-assembling deposition of poly-L-lysine and trichloro(1*H*,1*H*,2*H*,2*H*-perfluorooctyl) silane solutions, respectively. Using this method, the TEG with P-PET:F-PET pair showed high V_{oc} of ∼330 V and J_{sc} of ∼270 mA/m^2, which also exhibited outstanding stability over long period of measurement. Further improvement in output power is expected by applying the method on the device with surface patterns. The method demonstrated here provides simple, effective, and cost-competitive to fabricate high performance TEGs.

EXPERIMENTAL METHOD

Surface Functionalization. The ITO (100 nm) coated PET substrates (Sigma-Aldrich) were cleaned by acetone, isopropyl alcohol (IPA), and DI water, followed by treatment in oxygen plasma (O_2, 8 sccm; RF Power, 80 W; *t*, 100 s). For the surface functionalization, the prepared PET substrate was soaked in a glass container for 5 min, containing poly-L-lysine solution (0.1% in H_2O, Sigma-Aldrich). Subsequently, the poly-L-lysine coated PET substrate was washed with DI water and blow-dried with N_2. The other PET substrate was put in a sealed container by dropping few trichloro(1*H*,1*H*,2*H*,2*H*-perfluorooctyl) silane (FOTS) drops (97%, Sigma-Aldrich) and was placed in an oven for 95 °C for 1 h.

Characterization. The output voltage and current were measured by using an oscilloscope (LeCroy, LT354) and current preamplifier (Stanford Research Systems, SR 570), respectively. The cyclic contact and retraction motions were performed by a custom-built push machine setup. A contact angle analyzer (Surface Electro Optics, Phoenix300) was used to measure the water contact angles of functionalized PET surfaces.

Conflict of Interest: The authors declare no competing financial interest.

Acknowledgment. This research was supported by Basic Science Research Program through the National Research Foundation of Korea (NRF-2012R1A1A1041869).

Supporting Information Available: The additional figures include the TEG output performance under reserve connection mode, output performance of the TEG with PET:H-PET pair and H-PET:F-PET pair, rectified output voltage and current of the TEG with P-PET:F-PET pair, and schematic drawing of the bride rectifier circuit. The additional movie file include lighting up of blue LEDs during pressing/releasing motions. This material is available free of charge *via* the Internet at http://pubs.acs.org.

REFERENCES AND NOTES

1. Hudson, M. The Final Energy Crisis. *Environ. Pollut.* **2006**, *15*, 677–679.
2. Wang, Z. L.; Wu, W. Nanotechnology-Enabled Energy Harvesting for Self-Powered Micro-/Nanosystems. *Angew. Chem., Int. Ed.* **2012**, *51*, 2–24.
3. Aricò, A. S.; Bruce, P.; Scrosati, B.; Tarascon, J.-M.; van Schalkwijk, W. Nanostructured Materials for Advanced Energy Conversion and Storage Devices. *Nat. Mater.* **2005**, *4*, 366–377.
4. Dresslhaus, M. S.; Tomas, I. L. Alternative Energy Technologies. *Nature* **2001**, *414*, 332–337.
5. Xu, S.; Qin, Y.; Xu, C.; Wei, Y.; Wang, R.; Wang, Z. L. Self-Powered Nanowire Devices. *Nat. Nanotechnol.* **2010**, *5*, 366–373.
6. Mitcheson, P. D.; Yeatman, E. M.; Rao, G. K.; Holmes, A. S.; Green, T. C. Energy Harvesting from Human and Machine Motion for Wireless Electronic Devices. *Proc. IEEE* **2008**, *96*, 1457–1486.
7. Cheng, G.; Lin, Z.-H.; Du, Z.-l.; Wang, Z. L. Simultaneously Harvesting Electrostatic and Mechanical Energies from Flowing Water by a Hybridized Triboelectric Nanogenerator. *ACS Nano* **2014**, *8*, 1932–1939.
8. Williams, C. B.; Shearwood, C.; Harradine, M. A.; Mellor, P. H.; Birch, T. S.; Yates, R. B. Development of an Electromagnetic Micro-Generator. *Proc. IEEE Circ. Dev. Syst.* **2001**, *148*, 337–342.
9. Miller, M. M.; Prinz, G. A.; Lubitz, P.; Hoines, L.; Krebs, J. J.; Cheng, S. F.; Parsons, F. G. Novel Absolute Linear Displacement Sensor Utilizing Giant Magnetoresistance Elements. *J. Appl. Phys.* **1997**, *81*, 4284–4286.
10. Beeby, S. P.; Torah, R. N.; Tudor, M. J.; Glynne-Jones, P.; O'Donnell, T.; Saha, C. R.; Roy, S. A Micro Electromagnetic Generator for Vibration Energy Harvesting. *J. Micromech. Microeng.* **2007**, *17*, 1257–1265.
11. Shin, S.-H.; Kim, Y.-H.; Lee, M. H.; Jung, J.-Y.; Nah, J. Hemispherically Aggregated $BaTiO_3$ Nanoparticle Composite Thin Film for High-Performance Flexible Piezoelectric Nanogenerator. *ACS Nano* **2014**, *8*, 2766–2773.
12. Chen, X.; Xu, S.; Yao, N.; Shi, Y. 1.6 V Nanogenerator for Mechanical Energy Harvesting Using PZT Nanofibers. *ACS Nano* **2010**, *10*, 2133–2137.
13. Gupta, M. K.; Lee, J.-H.; Lee, K. Y.; Kim, S.-W. Two-Dimensional Vanadium-Doped ZnO Nanosheet-Based Flexible Direct Current Nanogenerator. *ACS Nano* **2013**, *7*, 8932–8939.
14. Shin, S.-H.; Kim, Y.-H.; Lee, M. H.; Jung, J.-Y.; Seol, J. H.; Nah, J. Lithium-Doped Zinc Oxide Nanowires−Polymer Composite

for High Performance Flexible Piezoelectric Nanogenerator. *ACS Nano* **2014**, *8*, 10844–10850.
15. Shin, S.-H.; Lee, M. H.; Jung, J.-Y.; Seol, J. H.; Nah, J. Piezoelectric Performance Enhancement of ZnO Flexible Nanogenerator by a CuO−ZnO P−N Junction Formation. *J. Mater. Chem. C* **2013**, *1*, 8103–8107.
16. Pelrine, R.; Kornbluh, R. D.; Eckerle, J.; Jeuck, P.; Oh, S.; Pei, Q.; Stanford, S. Dielectric Elastomers: Generator Mode Fundamentals and Applications. *Proc. SPIE* **2001**, *4329*, 148–156.
17. Mitcheson, P. D.; Miao, P.; Stark, B. H.; Yeatman, E. M.; Holmes, A. S.; Green, T. C. MEMS Electrostatic Micro-Power Generator for Low Frequency Operation. *Sens. Actuators, A* **2004**, *115*, 523–529.
18. Baytekin, H. T.; Patashinski, A. Z.; Branicki, M.; Baytekin, B.; Soh, S.; Grzybowski, B. A. The Mosaic of Surface Charge in Contact Electrification. *Nature* **2011**, *333*, 308–312.
19. Niu, S.; Wang, S.; Lin, L.; Liu, Y.; Zhou, Y. S.; Hu, Y.; Wang, Z. L. Theoretical Study of Contact-Mode Triboelectric Nanogenerators as an Effective Power Source. *Energy Environ. Sci.* **2013**, *6*, 3576–3583.
20. Zhang, X.-S.; Han, M.-D.; Wang, R.-X.; Zhu, F.-Y.; Li, Z.-H.; Wang, W.; Zhang, H.-X. Frequency-Multiplication High-Output Triboelectric Nanogenerator for Sustainably Powering Biomedical Microsystems. *Nano Lett.* **2013**, *13*, 1168–1172.
21. Fan, F.-R.; Tian, Z.-Q.; Wang, Z. L. Flexible Triboelectric Generator. *Nano Energy* **2012**, *1*, 328–334.
22. Wang, S.; Lin, L.; Wang, Z. L. Triboelectric Nanogenerators as Self-Powered Active Sensors. *Nano Energy* **2015**, *11*, 436–462.
23. Fan, F.-R.; Lin, L.; Zhu, G.; Wu, W.; Zhang, R.; Wang, Z. L. Transparent Triboelectric Nanogenerators and Self-Powered Pressure Sensors Based on Micropatterned Plastic Films. *Nano Lett.* **2012**, *12*, 3109–3114.
24. Zhu, G.; Pan, C.; Guo, W.; Chen, C.-Y.; Zhou, Y.; Yu, R.; Wang, Z. L. Triboelectric-Generator-Driven Pulse Electrodeposition for Micropatterning. *Nano Lett.* **2012**, *12*, 4960–4965.
25. Lee, K. Y.; Chun, J.; Lee, J.-H.; Kim, K. N.; Kang, N.-R.; Kim, J.-Y.; Kim, M. H.; Shin, K.-S.; Gupta, M. K.; Baik, J. M.; et al. Hydrophobic Sponge Structure-Based Triboelectric Nanogenerator. *Adv. Mater.* **2014**, *26*, 5037–5042.
26. Jeong, C. K.; Baek, K. M.; Niu, S.; Nam, T. W.; Hur, Y. H.; Park, D. Y.; Hwang, G.-T.; Byun, M.; Wang, Z. L.; Jung, Y. S.; et al. *Nano Lett.* **2014**, *14*, 7031–7038.
27. Wen, X.; Yang, W.; Jing, Q.; Wang, Z. L. Harvesting Broadband Kinetic Impact Energy from Mechanical Triggering/Vibration and Water Waves. *ACS Nano* **2014**, *8*, 7405–7412.
28. Bai, P.; Zhu, G.; Liu, Y.; Chen, J.; Jing, Q.; Yang, W.; Ma, J.; Zhang, G.; Wang, Z. L. Cylindrical Rotating Triboelectric Nanogenerator. *ACS Nano* **2013**, *7*, 6361–6366.
29. Xie, Y.; Wang, S.; Lin, L.; Jing, Q.; Lin, Z.-H.; Niu, S.; Wu, Z.; Wang, Z. L. Rotary Triboelectric Nanogenerator Based on a Hybridized Mechanism for Harvesting Wind Energy. *ACS Nano* **2013**, *7*, 7119–7125.
30. Jing, Q.; Zhu, G.; Bai, P.; Xie, Y.; Chen, J.; Han, Ray P. S.; Wang, Z. L. Case-Encapsulated Triboelectric Nanogenerator for Harvesting Energy from Reciprocating Sliding Motion. *ACS Nano* **2014**, *8*, 3836–3842.
31. Xie, Y.; Wang, S.; Niu, S.; Lin, L.; Jing, Q.; Yang, J.; Wu, Z.; Wang, Z. L. Grating-Structured Freestanding Triboelectric-Layer Nanogenerator for Harvesting Mechanical Energy at 85% Total Conversion Efficiency. *Adv. Mater.* **2014**, *26*, 6599–6607.
32. Kuvaldina, E. V.; Rybkin, V. V.; Titov, V. A.; Shutov, D. A. Kinetics of Structural and Chemical Changes in Poly(ethylene terephthalate) Films Treated in Oxygen and Nitrogen Plasmas. *High Energy Chem.* **2005**, *39*, 397–402.
33. Wolf, R.; Sparavigna, A. C. Role of Plasma Surface Treatments on Wetting and Adhesion. *Engineering* **2010**, *2*, 342–345.
34. Zhuang, Y. X.; Hansen, O.; Knieling, T.; Wang, C.; Rombach, P.; Lang, W.; Benecke, W.; Kehlenbeck, M.; Koblitz, J. Vapor-Phase Self-Assembled Monolayers for Anti-Stiction Applications in MEMS. *J. Microelectromech. Syst.* **2007**, *16*, 1451–1460.
35. Rainaldi, G.; Calcabrini, A.; Santini, M. T. Positively Charged Polymer Polylysine-Induced Cell Adhesion Molecule Redistribution in K562 Cells. *J. Mater. Sci. Mater. Med.* **1998**, *9*, 755–760.
36. Yamamoto, H.; Ogawa, T.; Nishida, A. Molecular Weight Dependence of Wettability and Molecular Adsorption of Poly-$_L$-Lysine at the Air−Water Interface. *J. Colloid Interface Sci.* **1995**, *176*, 105–110.
37. Khatri, O. P.; Devaprakasam, D.; Biswas, S. K. Frictional Responses of Octadecyltrichlorosilane (OTS) and 1H, 1H, 2H, 2H-Perfluorooctyltrichlorosilane (FOTS) Monolayers Self-Assembled on Aluminium over Six Orders of Contact Length Scale. *Tribol. Lett.* **2005**, *20*, 235–246.